IEEE Access
Multidisciplinary ⋮ Rapid Review ⋮ Open Access Journal

Received May 12, 2021, accepted June 24, 2021, date of publication July 6, 2021, date of current version July 13, 2021.

Digital Object Identifier 10.1109/ACCESS.2021.3095065

A Two-Dimensional Direction Finding Method Based on Non-Uniform Array

GUIBAO WANG[1], PEIYAO ZHAO[2], LE WANG[3], AND LANMEI WANG[3]
[1]School of Physics and Telecommunication Engineering, Shaanxi University of Technology, Hanzhong 723001, China
[2]School of Telecommunications Engineering, Xidian University, Xi'an 710071, China
[3]School of Physics and Optoelectronic Engineering, Xidian University, Xi'an 710071, China

Corresponding author: Lanmei Wang (lmwang@mail.xidian.edu.cn)

This work was supported in part by the National Natural Science Foundation of China under Grant 61772398 and Grant 61972239, in part by the Key Research and Development Program Projects of Shaanxi Province under Grant 2019SF-257, Grant 2020GY-024, and Grant 2021GY-182; and in part by the Science and Technology Program of Hantai District under Grant 2019KX-21.

ABSTRACT In this paper, an aperture expanding direction finding algorithm using L-shaped non-uniform sparse array is proposed. Firstly, the virtual array is expanded by vectorizing, de-redundant and sorting of received data covariance matrix. Secondly, the full rank matrix is got by smoothing the virtual array data, and the signal subspace is obtained by matrix block processing. Finally, the elevation angle and azimuth angle are acquired by using the rotation invariant relation. The algorithm does not need to decompose the covariance matrix of the data, nor does it need to search the two-dimensional spectral peaks. It can greatly reduce the computational complexity when there are many array elements and large number of snapshots. The simulation results show that the sparse array arrangement can enlarge the array aperture, improve the parameter resolution and the accuracy of DOA estimation, and verify the effectiveness of the proposed algorithm.

INDEX TERMS Extended ESPRIT method, non-uniform array, direction finding, L-shaped array, sparse array.

I. INTRODUCTION

In far-field cases, the array steering vector matrix of uniform linear array is Vandermonde matrix, traditional direction of arrival (DOA) estimation algorithms, such as ESPRIT and forward-backward spatial smoothing algorithms, can be realized in the uniform linear array. The received signal of a line array is only a one-dimensional function of the DOA, it is easy to realize parameter estimation without dimension reduction, pairing, and other operations. Therefore, the uniform linear array is widely used in signal location algorithm. In order to improve the accuracy of angle estimation, the traditional full array generally requires a large number of sensor elements to expand the effective aperture of the array, which requires a large number of hardware devices such as sensors and samplers, resulting in a significant increase in system operation and maintenance costs and operational complexity [1]–[3]. When the array aperture is constant, the non-uniform array can effectively reduce the array element number and implementation costs, therefore, it is widely used. The coprime array can enlarge the array aperture [4], [5]. In [4], a two-dimensional direction-of-departure and DOA estimation for bistatic multiple-input multiple-output radar was proposed by introducing an improved higher order singular value decomposition estimator and using a coprime electromagnetic vector sensor, and a tensor-based subspace algorithm is proposed. In 2010s a nested array structure was proposed in [6]–[8]. In [9], a multi-level nested array was proposed by extending the standard two-level nested array. In [10], an extended two-level nested array was proposed, this type of array structure expanded the array aperture and improved the DOA estimation accuracy by vectorizing the received covariance data of the array and using a virtual array instead of an original array. However, the common defect is that, in this method, each subarray is composed of a uniform linear subarray, which often leads to the problem that it is unable to find a reasonable location for the subarray element installation in the actual engineering installation process when the airborne radar or physical space is limited. For this reason, in [11],

The associate editor coordinating the review of this manuscript and approving it for publication was Weiren Zhu.

a kind of array with the same performance as the nested array was designed, with a more flexible array arrangement.

When the signal propagates in three-dimensional space, the linear array has obvious defects regarding the signal source location. As shown in Figure 1, the signal is incident along any direction of the cone with an angle of θ from the x-axis. The received data of the linear array is exactly the same, and the linear array cannot distinguish the true signal direction. Therefore, when the linear array is used to locate the signal source, the incident direction is limited in the xoz plane, and the application range of the linear array is severely limited [12]. A two-dimensional array can distinguish the direction of the signal from three-dimensional space. Two-dimensional DOA estimation based on the two-dimensional array has been able to obtain more target position information (elevation and azimuth) than one-dimensional DOA estimation, so it has attracted people's attention. The uniform L-shaped array is often used as the receiving array in the traditional two-dimensional DOA estimation methods. With the development of science and technology, higher and higher requirements are put forward for the accuracy of parameter estimation. The traditional method no longer meets the requirements of the accuracy and resolution of parameter estimation. In recent years, non-uniform sparse L-shaped array emerges and develops rapidly.

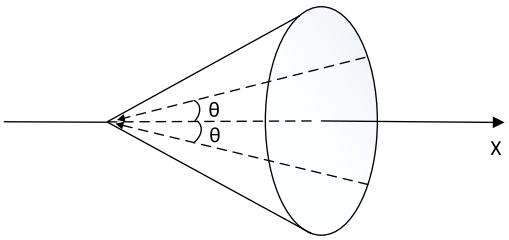

FIGURE 1. Schematic diagram of the signal incident to the linear array.

Two-dimensional super-resolution methods, such as the multiple signal classification (MUSIC) [13], [14], estimation of signal parameters via rotational invariance techniques (ESPRIT) [15], [16], and the two-dimensional Root-MUSIC [17] and its derivative algorithm [18], [19] are used. When the two-dimensional MUSIC algorithm is used to search the two-dimensional spectrum, a high storage space and fast computer processing are required, so it is not conducive to engineering implementation. Although the two-dimensional ESPRIT algorithm does not need to search the spectrum, it needs to solve the covariance matrix (CM) of the received data and carry out the eigenvalue decomposition (EVD). Therefore, in the case of having many array elements and a large number of snapshots, the amount of calculation from the ESPRIT algorithm to solve the CM and EVD operations will increase significantly. In recent years, new two-dimensional DOA estimation methods based on the L-shaped array have been proposed [20]–[31], such as the joint singular value decomposition (JSVD) algorithm [20], the cross correlation matrix ESPRIT (CCM-ESPRIT) algorithm [21], the joint angle estimation algorithm for finding the root of polynomials [22], and the improved PM algorithm for two-dimensional L-shaped arrays [23]. In [24], an algorithm that uses two parallel nested arrays was proposed. A method that can effectively estimate the coherent signal received by the coprime array is proposed in [25], which uses the Toeplitz matrix and the nuclear norm minimization problem to analyze the coherent signal. In reference to the DOA estimation problem of a two-dimensional coprime planar array, Lu proposed a meshless sparse reconstruction algorithm using decoupled atomic norm minimization theory, which reduces the complexity of the algorithm [26]. In [27], a fast-convergent trilinear decomposition method is applied to the two-dimensional DOA estimation of multiple signals of a generalized coprime planar array composed of two rectangular uniform planar sub-arrays, which has good estimation performance. However, the two-dimensional Root-MUSIC algorithm, the joint angle estimation algorithm for finding the root of polynomials, and the CCM-ESPRIT algorithm require the eigen-decomposition of the covariance matrix. Moreover, the CCM-ESPRIT algorithm still has the problem of pairing failure when the signal-to-noise ratio (SNR) is low. The JSVD algorithm not only needs the SVD but also uses spectrum search to solve the azimuth, which has high complexity.

Compared with the uniform array, the non-uniform array such as nested array and coprime array enlarges the array aperture and improves the array freedom. However, the sub-array of nested array and coprime array is uniform array, which affects the flexibility of array layout. For aircraft and other special platform with limited array layout, it is of great significance to study a more flexible non-uniform array. For this reason, this paper expands the non-uniform linear array [11] into a two-dimensional non-uniform L-shaped array, and changes the one-dimensional DOA estimation into a joint estimation of the spatial azimuth and elevation, which makes up for the lack of spatial azimuth information in the linear array DOA estimation and is more similar to the practical engineering application. In this paper, the definitions of the azimuth and elevation are different from those presented in the literature [20]–[22], the angle parameters of the x-axis and z-axis are decoupled, and there is no error accumulation in the parameter estimation of the two directions. Hence, the array manifold matrix of the x-axis subarray changes from the traditional cosine relationship of the azimuth and elevation to that of the azimuth only. The array manifold matrix of the z-axis subarray is only related to the elevation. The two-dimensional parameter estimation of the x-axis subarray is herein changed into one-dimensional parameter estimation, which realizes the parameter dimensionality reduction and lays the foundation for the improvement of the subsequent estimation accuracy and calculation amount. In order to avoid the high computational complexity caused by eigen-decomposition and spectrum search, a new two-dimensional DOA estimation algorithm is proposed, which constructs an auxiliary operator to obtain the signal

subspace and obtains the elevation and azimuth through the improved ESPRIT-based algorithm. The simulation results show that this method has higher spatial resolution and parameter estimation accuracy than the existing method.

II. NON-UNIFORM L-SHAPED ARRAY STRUCTURE

The nested array can obtain the maximum degree of freedom (DOF), that is, the maximum number of virtual elements [6]. According to the maximum number of virtual elements, the position coefficients of the first and last elements of the non-uniform array are determined, and the residual element position coefficients of the non-uniform array are also calculated. The non-uniform array is constructed based on the position coefficient of the array element. For convenience of description, the x-axis and z-axis subarrays are two-level nested arrays with an even number of array elements, that is, the number of array elements N and M are even. The case where N and M are odd numbers can be obtained by analogy. Next, we take the x-axis subarray as an example to illustrate the specific steps:

(1) The position coefficients $n_1 = 0$ and $n_N = \tilde{N}$ of a non-uniform array are determined based on the maximum DOF D_F of the nested array, where $\tilde{N} = (D_F - 1)/2$ and $D_F = 2N_2(N_1+1)-1$. N_1 and N_2 are the number of subarray elements in the nested arrays and $N_1 + N_2 = N$. Where $D = d \times [n_1, \ldots, n_n, \ldots, n_N]$ is the array element position of the nonuniform array, the interval of elements d is half-wavelength spacing, n_n denotes the position coefficient of the n-th elements of the nonuniform array, $n = 1, 2, \ldots, N$, n_1 and n_N represent the position coefficient of the first and N-th elements of the nonuniform array.

(2) Randomly select $N - 2$ different natural numbers arranged in ascending order to form an array $[n_2, \ldots, n_n, \ldots, n_{N-1}]$, construct the element position $\boldsymbol{\Omega} = [\xi_1, \ldots, \xi_n, \ldots, \xi_N] = [0, n_2, \ldots, n_n, \ldots, n_{N-1}, \tilde{N}]\lambda/2$ of the non-uniform array, where λ is the incident signal wavelength, the elements of $\tilde{\mathbf{n}} = [n_2, \ldots, n_n, \ldots, n_{N-1}]$ are the random increasing natural integers, and the value range of $\tilde{\mathbf{n}}$ is $\tilde{\mathbf{n}} \in [1, \tilde{\mathrm{N}} - 1]$.

(3) Construct the matrix $\bar{\mathbf{P}}$ of $N \times N$, i. e.,

$$\bar{\mathbf{P}} = [(\boldsymbol{\Omega} - \xi_1\mathbf{h})^{\mathrm{T}}, (\boldsymbol{\Omega} - \xi_2\mathbf{h})^{\mathrm{T}}, \ldots, (\boldsymbol{\Omega} - \xi_N\mathbf{h})^{\mathrm{T}}] \quad (1)$$

where $\mathbf{h}$ is the all 1 matrix of $1 \times \mathrm{N}$, $(\cdot)^{\mathrm{T}}$ represents the transpose operation.

As shown by equation (1), $\bar{\mathbf{P}}$ is an anti-symmetric matrix. If $\bar{\mathbf{P}}$ is complete, the array $[n_2, \ldots, n_n, \ldots, n_{N-1}]$ in step (2) is the actual position coefficient of non-uniform array elements, so rename it $[\tilde{n}_2, \ldots, \tilde{n}_n, \ldots, \tilde{n}_{N-1}]$, and the non-uniform array position is $\tilde{\boldsymbol{\Omega}} = [\tilde{\xi}_1, \tilde{\xi}_2, \ldots, \tilde{\xi}_n, \ldots, \tilde{\xi}_N]$, i. e., $\tilde{\boldsymbol{\Omega}} = [0, \tilde{n}_2, \ldots, \tilde{n}_n, \ldots, \tilde{n}_{N-1}, \tilde{N}]\lambda/2$.

(4) If the matrix $\bar{\mathbf{P}}$ obtained in step (3) is not complete, go back to step (2) and carry out iterations until the iteration stop condition that $\bar{\mathbf{P}}$ is complete is met. Then, the iteration is exited.

The derivation process of the above method is detailed in [11]. According to the obtained array element position, the L-shaped array is arranged in the positive direction in the x-axis and z-axis.

III. SIGNAL MODEL

According to the method presented in Section II, the element position $\tilde{\Omega}$ is obtained. The array is arranged along the x-axis and z-axis according to the element position $\tilde{\Omega}$. The two subarrays have N and M elements, respectively. The "0" element at the origin is shared by the two subarrays as the reference element. We suppose K uncorrelated far-field narrow-band signals are incident on the proposed L-shaped array shown in Figure 2.

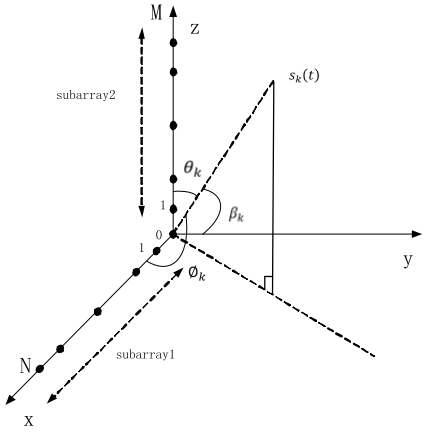

FIGURE 2. Non-uniform L-shaped array structure (M = N = 6).

Let $x_n(t)$ and $z_m(t)$ be the signals received by the n-th element of the x-axis and the m-th element of the z-axis, respectively. Then, the received data vector of the x-axis and z-axis arrays at time t are represented as $\mathbf{z}(t) = [z_1(t), \ldots, z_m(t), \ldots, z_M(t)]^{\mathrm{T}}$ and $\mathbf{x}(t) = [x_1(t), \ldots, x_n(t), \ldots, x_N(t)]^{\mathrm{T}}$, where $t = \{1, 2, \ldots, L\}$, L represents the number of snapshots. Suppose $s_k(t)$ is the signal of the k-th target source, the signals of the K target sources are represented as $\mathbf{s}(t) = [s_1(t), \ldots, s_k(t), \ldots, s_K(t)]^{\mathrm{T}}$

A. DEFINITION OF THE TRADITIONAL SIGNAL DOA

The traditional definition of the signal DOA is shown in Figure 3. $\theta_k \in [0, \pi]$ indicates the signal's elevation measured from the vertical z-axis, and $\tilde{\phi}_k \in [-\pi, \pi]$ denotes the azimuth measured from the positive x-axis. The array manifold of the x-axis array can be expressed as $\boldsymbol{a}_x(\theta_k, \tilde{\phi}_k) = [1, \mathrm{e}^{-\mathrm{j}\frac{2\pi}{\lambda}d_2\sin\theta_k\cos\tilde{\phi}_k}, \ldots, \mathrm{e}^{-\mathrm{j}\frac{2\pi}{\lambda}d_n\sin\theta_k\cos\tilde{\phi}_k}, \ldots, \mathrm{e}^{-\mathrm{j}\frac{2\pi}{\lambda}d_N\sin\theta_k\cos\tilde{\phi}_k}]^{\mathrm{T}}$, $n = 2, \ldots, N$, where d_n denotes the position coordinates of the n-th array element on the x-axis, λ indicates the incident signal wavelength, and $(\cdot)^{\mathrm{T}}$ represents the transpose operation. From the expression of the array manifold, it can be seen that the elevation θ_k and azimuth $\tilde{\phi}_k$ are coupled. This brings many problems for the subsequent parameter estimation, for example, the MUSIC peak search is a two-dimensional search, and the ESPRIT algorithm has error accumulation. In [20]–[22], the traditional definition of

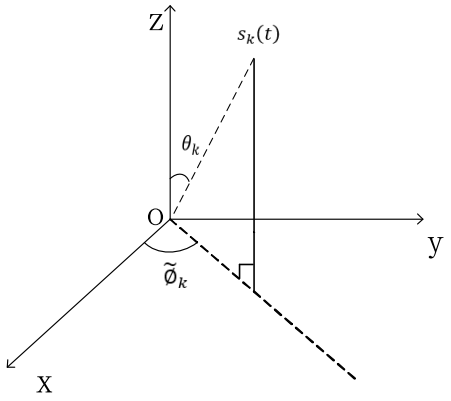

FIGURE 3. Definition of the traditional signal DOA.

the DOA is adopted. From the simulation results in Section VI of this paper, it can be seen that the accuracy of the azimuth estimation is poor due to the accumulation of errors.

B. THE PROPOSED DOA DEFINITION

The definition of the signal DOA in this paper is shown in Figure 2. The elevation $\theta_k \in [0, \pi]$ is the angle between the k-th incident signal and the positive z-axis, which is the same as the traditional definition. The azimuth $\phi_k \in [0, \pi]$ is the angle between the k-th incident signal and the positive x-axis, which is different from the traditional definition. β_k is the angle between the k-th incident signal and the positive y-axis. Because $\cos^2\theta_k + \cos^2\phi_k + \cos^2\beta_k = 1$, (θ_k, ϕ_k) can also uniquely determine the direction of the k-th signal, there is a certain transformation relationship for $\cos\phi_k = \sin\theta_k\cos\tilde{\phi}_k$ between the traditional definition and the proposed definition. In this way, the angle parameters of the x-axis and z-axis are decoupled, and there is no error accumulation in the parameter estimation of the two directions. The array mani-folds can be expressed as $\mathbf{A}(\phi) = [\mathbf{a}(\phi_1), \ldots, \mathbf{a}(\phi_k), \ldots, \mathbf{a}(\phi_K)]$ and $\mathbf{G}(\theta) = [\mathbf{g}(\theta_1), \ldots, \mathbf{g}(\theta_k), \ldots, \mathbf{g}(\theta_K)]$, where $k = 1, 2, \ldots, K$, K represents the total number of incident targets, $\mathbf{a}(\phi_k) = [1, \mathrm{e}^{-\mathrm{j}2\pi d_2 \cos\phi_k/\lambda}, \ldots, \mathrm{e}^{-\mathrm{j}2\pi d_n \cos\phi_k/\lambda}, \ldots, \mathrm{e}^{-\mathrm{j}2\pi d_N \cos\phi_k/\lambda}]^{\mathrm{T}}$ and $\mathbf{g}(\theta_k) = [1, \ldots, \mathrm{e}^{-\mathrm{j}2\pi d_m \cos\theta_k/\lambda}, \ldots, \mathrm{e}^{-\mathrm{j}2\pi d_{\mathrm{M}} \cos\theta_k/\lambda}]^{\mathrm{T}}$ represent the steering vector of the k-th incident target, $(\cdot)^{\mathrm{T}}$ represents the transpose operation, λ is the incident signal wavelength, and d_n and d_m represent the n-th and m-th element positions of the two subarrays. In summary, the received signal model is expressed as follows:

$$\mathbf{x}(t) = \mathbf{A}(\phi)\mathbf{s}(t) + \mathbf{n}_x(t) \tag{2}$$

$$\mathbf{z}(t) = \mathbf{G}(\theta)\mathbf{s}(t) + \mathbf{n}_z(t) \tag{3}$$

where $\mathbf{n}_x(t)$ and $\mathbf{n}_z(t)$ represent the complex Gaussian white noise with a mean of 0 and a variance of δ_n^2, in addition, $\mathbf{n}_x(t)$, $\mathbf{n}_z(t)$ and incident signal are independent of each other.

From the above definition, the received data covariance matrix of the x-axis sub-array can be obtained as

$$\mathbf{R}_x = \mathrm{E}[\mathbf{x}(t)\mathbf{x}^{\mathrm{H}}(t)] \in \mathbf{C}^{N\times N} \tag{4}$$

where $\mathrm{E}[\cdot]$ means to solve mathematical expectations, $(\cdot)^{\mathrm{H}}$ denotes the conjugate transpose operation, and the above formula can be simplified as follows:

$$\mathbf{R}_x = \mathbf{A}\mathbf{R}_{\mathrm{ss}}\mathbf{A}^{\mathrm{H}} + \mathbf{R}_N \tag{5}$$

where $\mathbf{R}_{\mathrm{ss}}$ and $\mathbf{R}_{\mathrm{N}}$ are the covariance matrix of the signal and noise, respectively, with

$$\mathbf{R}_{\mathrm{ss}} = \mathrm{diag}(\sigma_1^2, \ldots, \sigma_k^2, \ldots, \sigma_K^2) \tag{6}$$

$$\mathbf{R}_{\mathrm{N}} = \delta_n^2\mathbf{\Sigma}_{\mathrm{N}} \tag{7}$$

where $\mathrm{diag}(\cdot)$ represents the transformation of a vector matrix into a diagonal matrix, σ_k^2 is the power of the k-th incident signal, δ_n^2 is the power of the noise, and $\mathbf{\Sigma}_{\mathrm{N}}$ is the unit matrix of $\mathrm{N} \times \mathrm{N}$.

By vectorizing the covariance matrix of the received data of the x-axis sub array, the received data matrix of the virtual differential synthetic array (including the repeated array elements) is obtained:

$$\mathbf{r}_x = \mathrm{vec}(\mathbf{R}_x) = (\mathbf{A}^*(\phi) \odot \mathbf{A}(\phi))\mathbf{r}_p + \delta_n^2\mathbf{I}_n. \tag{8}$$

Similar to the process of getting the receiving data matrix of the virtual differential synthetic array from the x-axis, the z-axis data matrix can be obtained quickly:

$$\mathbf{r}_z = \mathrm{vec}(\mathbf{R}_z) = (\mathbf{G}^*(\theta) \odot \mathbf{G}(\theta))\mathbf{r}_p + \delta_n^2\mathbf{I}_m \tag{9}$$

where $\mathrm{vec}(\bullet)$ represents the vectorization operation on the matrix, $(\cdot)^*$ is the conjugate operation, $\odot$ denotes the Khatri–Rao product operation [24], $\mathbf{r}_p = [\sigma_1^2, \ldots, \sigma_k^2, \ldots, \sigma_K^2]^{\mathrm{T}}$, $\mathbf{I}_n = [\mathrm{e}_1^{\mathrm{T}}, \mathrm{e}_2^{\mathrm{T}}, \ldots, \mathrm{e}_N^{\mathrm{T}}]^{\mathrm{T}}$, $\mathbf{I}_m = [\mathrm{e}_1^{\mathrm{T}}, \mathrm{e}_2^{\mathrm{T}}, \ldots, \mathrm{e}_M^{\mathrm{T}}]^{\mathrm{T}}$, $\mathbf{r}_x \in \mathbf{C}^{N^2\times 1}$, $\mathbf{r}_z \in \mathbf{C}^{M^2\times 1}$, and $\mathbf{e}_i = [0, \ldots, 1, 0, \ldots, 0]^{\mathrm{T}}$ is a column vector, which is 1 only in the i-th position and 0 in the rest position, $i = 1, 2, \ldots, \max(N, M)$.

IV. DATA PROCESSING RECEIVED BY EACH SUBARRAY

The data output from the x-axis subarray is vectorized to obtain the virtual differential synthesis array receiving data $\mathbf{r}_x$. Because $\mathbf{r}_x$ contains repeated virtual array element data, $\mathbf{r}_x$ cannot be directly used as input data for the DOA estimation algorithm, and data processing (de-redundancy, sorting) operations are first needed to get the x-axis virtual array receiving data $\hat{\mathbf{r}}_x$. According to equation (8), it can be known that the received data $\mathbf{r}_x$ contains noise, and it is impossible to directly perform de-redundancy and sort operations on $\mathbf{r}_x$. However, the positions of the array element of the received data matrix $\mathbf{r}_x$ correspond to the positions of the differential array elements generated by the x-axis subarray. The index set is obtained by processing the positions of the differential array elements. The inner elements of $\mathbf{r}_x$ can be selected by the index set to sort and make de-redundant $\mathbf{r}_x$, and $\hat{\mathbf{r}}_x$ is herein obtained. The specific steps are as follows:

(1) According to the non-uniform array obtained in this paper, the column vector $\tilde{\mathbf{P}}$ can be constructed. It can be

expressed as the following formula (10):

$$\begin{aligned}\tilde{\mathbf{p}} &= [\tilde{p}_1, \ldots, \tilde{p}_i, \ldots, \tilde{p}_{N^2}]^{\mathrm{T}} \\ &= [(\tilde{\boldsymbol{\Omega}} - \tilde{\xi}_1\mathbf{h}), (\tilde{\boldsymbol{\Omega}} - \tilde{\xi}_2\mathbf{h}), \ldots, (\tilde{\boldsymbol{\Omega}} - \tilde{\xi}_N\mathbf{h})]^{\mathrm{T}} \end{aligned} \quad (10)$$

The position matrix of the uniform array composed of $2\tilde{N}+1$ elements with a half wavelength interval is the same as the virtual array element position matrix, which is expressed by vector $\mathbf{u}$. The expression of $\mathbf{u}$ can be expressed as follows:

$$\begin{aligned}\mathbf{u} &= [u_1, u_2, \ldots, u_j, \ldots, u_{2\tilde{N}+1}]^{\mathrm{T}} \\ &= [-\lambda\tilde{N}/2, \ldots, 0, \ldots, \lambda\tilde{N}/2]^{\mathrm{T}} \end{aligned} \quad (11)$$

The $2\tilde{N}+1$ elements of column vector $\tilde{\mathbf{p}}$ satisfying $\tilde{p}_i = u_j$ are selected to form a new vector $\hat{\mathbf{p}}$, and the position index set $\boldsymbol{\Gamma}$ of these $2\tilde{N}+1$ elements in $\tilde{\mathbf{p}}$ is recorded. According to the one-to-one correspondence between the element position of the received data $\mathbf{r}_x$ and the element position of the column vector $\tilde{\mathbf{p}}$, the index set $\boldsymbol{\Gamma}$ is used to select the useful data $\bar{\mathbf{r}}_x = \mathbf{r}_x(\boldsymbol{\Gamma})$ from the received data $\mathbf{r}_x$, so as to remove the redundant data, where $i = 1, 2, \ldots, N^2$, $j = 1, 2, \ldots, 2\tilde{N}+1$, $\tilde{\mathbf{p}} \in \mathbf{C}^{N^2\times 1}$, $\mathbf{u} \in \mathbf{C}^{(2\tilde{N}+1)\times 1}$, and $\hat{\mathbf{p}} \in \mathbf{C}^{(2\tilde{N}+1)\times 1}$.

(2) The new index set $\bar{\boldsymbol{\Gamma}}$ is obtained by sorting $\hat{\mathbf{p}}$, and the virtual array received data $\hat{\mathbf{r}}_x$ is obtained by sorting $\bar{\mathbf{r}}_x$ according to $\bar{\boldsymbol{\Gamma}}$.

The elements in $\hat{\mathbf{p}}$ are arranged in order from small to large, i.e., $[\mathbf{F}, \bar{\boldsymbol{\Gamma}}] = \mathrm{sort}(\hat{\mathbf{p}})$, and the sorted index set $\bar{\boldsymbol{\Gamma}}$ is obtained. The useful received data $\bar{\mathbf{r}}_x$ is sorted according to the index set $\bar{\boldsymbol{\Gamma}}$, and finally, the received data $\hat{\mathbf{r}}_x$ of the virtual array are obtained.

After the above de-redundancy and sorting, the received data of the virtual array are as follows:

$$\begin{aligned}\hat{\mathbf{r}}_x &= \bar{\mathbf{A}}(\phi)\mathbf{r}_p + \delta_n^2\mathbf{I}_{0n} \\ &= [\bar{\mathbf{a}}(\phi_1), \ldots, \bar{\mathbf{a}}(\phi_k), \ldots, \bar{\mathbf{a}}(\phi_K)] \\ &\quad \times [\sigma_1^2, \ldots, \sigma_k^2, \ldots, \sigma_K^2]^{\mathrm{T}} + \delta_n^2\mathbf{I}_{0n} \end{aligned} \quad (12)$$

where $\bar{\mathbf{a}}(\phi_k) = [\mathrm{e}^{-\mathrm{j}\frac{2\pi d}{\lambda}\cos\phi_k(-\tilde{N})}, \ldots, \mathrm{e}^{-\mathrm{j}\frac{2\pi d}{\lambda}\cos\phi_k(\tilde{N}-n)}, \ldots, \mathrm{e}^{-\mathrm{j}\frac{2\pi d}{\lambda}\cos\phi_k(\tilde{N})}]^{\mathrm{T}}, n = 1, 2, \ldots, \tilde{N}$, $\mathbf{I}_{0n}$ is a column vector whose $(\tilde{N}+1)th$ element is 1, and other elements are 0, $k = 1, 2, \ldots, K$.

It can be seen from equation (8) that after the Khatri–Rao product x-axis subarray, elements will be changed from N elements to $2\tilde{N}+1$ elements, i.e., $(N^2-2)/2+N$ elements.

Similar to the x-axis subarray data processing process, the z-axis subarray virtual array receiving data are obtained as follows:

$$\begin{aligned}\hat{\mathbf{r}}_z &= \bar{\mathbf{G}}(\theta)\mathbf{r}_p + \delta_n^2\mathbf{I}_{0m} \\ &= [\bar{\mathbf{g}}(\theta_1), \ldots, \bar{\mathbf{g}}(\theta_k), \ldots, \bar{\mathbf{g}}(\theta_K)] \\ &\quad \times [\sigma_1^2, \ldots, \sigma_k^2, \ldots, \sigma_K^2]^{\mathrm{T}} + \delta_n^2\mathbf{I}_{0m} \end{aligned} \quad (13)$$

where $\bar{\mathbf{g}}(\theta_k) = [\mathrm{e}^{-\mathrm{j}\frac{2\pi d}{\lambda}\cos\theta_k\left(-\tilde{M}\right)}, \ldots, \mathrm{e}^{-\mathrm{j}\frac{2\pi d}{\lambda}\cos\theta_k\left(\tilde{M}-m\right)}, \ldots, \mathrm{e}^{-\mathrm{j}\frac{2\pi d}{\lambda}\cos\theta_k\left(\tilde{M}\right)}]^{\mathrm{T}}, m = 1, 2, \ldots, \tilde{M}$. $\mathbf{I}_{0m}$ is a column vector whose $\left(\tilde{M}+1\right)th$ element is 1 and other elements are 0, with $\tilde{M} = (D_z - 1)/2$. $D_z = 2M_2(M_1 + 1) - 1$ is the number of virtual elements in the z-axis, and M_1 and M_2 are the numbers of z-axis subarray elements, respectively, which satisfy $M_1 + M_2 = \mathrm{M}$.

V. TWO-DIMENSIONAL DOA ESTIMATION ALGORITHM

In the case of a large number of antennas or sampling points, the calculation cost of the algorithms (such as ESPRIT, SVD, etc.) that need the eigen-decomposition operation will increase significantly, further increasing the actual application cost. To avoid this situation, an auxiliary operator is constructed for obtaining the signal subspace of each subarray, and selection matrices are defined in this section to get the target source elevation and azimuth, but the angle obtained at this time is disordered. Finally, the one-to-one corresponding elevation and azimuth angles are obtained by pairing algorithm.

A. ESTIMATION OF THE AZIMUTH AND ELEVATION

1) ESTIMATION OF THE AZIMUTH

According to the x-axis subarray virtual array received data $\hat{\mathbf{r}}_x$ described in the previous section, the array steering vector matrix $\bar{\mathbf{A}}(\phi)$ of $\hat{\mathbf{r}}_x$ is divided into $\bar{N}$ sub-matrixes. Each sub-matrix is represented by $\bar{\mathbf{A}}_i(\phi)$, and each $\bar{\mathbf{A}}_i(\phi)$ consists of rows i to $(\bar{N}+i-1)$ of matrix $\bar{\mathbf{A}}(\phi)$. For convenience of description, the noise term is temporarily removed from the formula expression. Then, it has the following expression:

$$\hat{\mathbf{r}}_i = \mathbf{J}_i\hat{\mathbf{r}}_x = \bar{\mathbf{A}}_i(\phi)\mathbf{r}_p \quad (14)$$

where $\mathbf{J}_i = [\mathbf{0}_{\bar{N},(i-1)}, \boldsymbol{\Sigma}_{\bar{N}}, \mathbf{0}_{\bar{N},(\bar{N}-i)}]$ is the selection matrix, $i = 1, \ldots, \bar{N}$, $\bar{N} = (D_F+1)/2$.

The full rank matrix $\mathbf{W}$ can be expressed as $\mathbf{W} = [\hat{\mathbf{r}}_1, \hat{\mathbf{r}}_2, \ldots, \hat{\mathbf{r}}_{\bar{N}}]$. In order to calculate the auxiliary operator $\mathbf{Q} \in \mathbf{C}^{K\times(\bar{N}-K)}$, the full rank matrix $\mathbf{W}$ is divided into $\mathbf{W} = [\mathbf{W}_1^{\mathrm{T}}, \mathbf{W}_2^{\mathrm{T}}]$, where $\mathbf{W}_1 \in \mathbf{C}^{K\times\bar{N}}$ is composed of the first K rows of $\mathbf{W}$, and $\mathbf{W}_2 \in \mathbf{C}^{(\bar{N}-K)\times\bar{N}}$ is composed of the $(\bar{N}-K)$ rows of $\mathbf{W}$.

The auxiliary operator can be calculated by the following formula.

$$\mathbf{Q} = (\mathbf{W}_1\mathbf{W}_1^{\mathrm{H}})^{-1}\mathbf{W}_1\mathbf{W}_2^{\mathrm{H}}. \quad (15)$$

According to the propagator method, the signal subspace $\mathbf{E}_S$ can be obtained as follows:

$$\mathbf{E}_S = \begin{bmatrix} \boldsymbol{\Sigma}_{\mathrm{K}} \\ \mathbf{Q}^{\mathrm{H}} \end{bmatrix} \quad (16)$$

where $\boldsymbol{\Sigma}_K$ is the identity matrix of $K \times K$, and $(\cdot)^{\mathrm{H}}$ denotes the conjugate transpose operation.

Define two selection matrices $\mathbf{J}_{g1}$ and $\mathbf{J}_{g2}$, i.e.,

$$\mathbf{J}_{g1} = [\boldsymbol{\Sigma}_{\bar{N}-1}, \mathbf{0}_{\bar{N}-1,1}] \quad (17)$$

$$\mathbf{J}_{g2} = [\mathbf{0}_{\bar{N}-1,1}, \boldsymbol{\Sigma}_{\bar{N}-1}] \quad (18)$$

where $\mathbf{J}_{g1} \in \mathbf{C}^{(\bar{N}-1)\times\bar{N}}$, $\mathbf{J}_{g2} \in \mathbf{C}^{(\bar{N}-1)\times\bar{N}}$, $\boldsymbol{\Sigma}_{\bar{N}-1}$ represents the identity matrix of $(\bar{N}-1)\times(\bar{N}-1)$, $\mathbf{0}_{\bar{N}-1,1}$ denotes the all-zero column vector of length $\bar{N}-1$.

According to the selection matrices $\mathbf{J}_{g1}$ and $\mathbf{J}_{g2}$, the signal subspaces $\mathbf{E}_{S1}$ and $\mathbf{E}_{S2}$ are obtained, that is, $\mathbf{E}_{S1} = \mathbf{J}_{g1}\mathbf{E}_S$ and $\mathbf{E}_{S2} = \mathbf{J}_{g2}\mathbf{E}_S$. Based on the improved ESPRIT-based method, the expression of $\mathbf{\Psi} = \mathbf{E}_{S1}^{\dagger}\mathbf{E}_{S2}$ is obtained by using the relationship between the signal subspaces $\mathbf{E}_{S1}$ and $\mathbf{E}_{S2}$, where $(\bullet)^{\dagger}$ represents the pseudo-inverse of the matrix. The eigen-decomposition of the matrix $\mathbf{\Psi} \in \mathbf{C}^{K\times K}$ is performed, that is, $[\mathbf{V}, \mathbf{U}_q] = \mathrm{eig}(\Psi)$, where $\mathbf{V}$ and $\mathbf{U}_q$ represent the eigen-vectors and eigenvalues of matrix $\mathbf{\Psi}$ respectively, $\mathrm{eig}(\cdot)$ represents the eigen- decomposition.

The estimated value of azimuth is as follows:

$$\hat{\phi}_k = \cos^{-1}\left[\frac{\arg(v_{kk})}{2\pi d/\lambda}\right] \tag{19}$$

where $\arg(\cdot)$ denotes the operation of returning the phase angles. v_{kk} is the element of the diagonal matrix $\mathbf{V}$ at row k and column k. If we let $\hat{\phi}_k = \hat{\phi}_{ak}$, the azimuth estimated values of K signals are $\hat{\mathbf{\Phi}} = [\hat{\phi}_{a1}, \ldots, \hat{\phi}_{ak}, \ldots, \hat{\phi}_{aK}]$.

2) ESTIMATION OF THE ELEVATION

The z-axis subarray and x-axis subarray have the same structure. According to formulas (12) and (13), it can be seen that the data structures of $\hat{\mathbf{r}}_x$ and $\hat{\mathbf{r}}_z$ are the same, and the function expressions of array manifolds $\mathbf{a}(\phi_k)$ and $\mathbf{g}(\theta_k)$ are similar with respect to ϕ_k and θ_k. Thus, similar to the azimuth estimation process, the elevation can be quickly estimated. The elevation estimated values of K signals are $\hat{\boldsymbol{\theta}} = [\hat{\theta}_{e1}, \ldots, \hat{\theta}_{ek}, \ldots, \hat{\theta}_{eK}]$.

However, the estimation of elevation $\hat{\theta}$ and estimation of azimuth $\hat{\phi}$ are out of order at this time. Through the pairing algorithm of the cross covariance matrix, the corresponding elevation and azimuth are obtained. The pairing process is as follows:

1) The estimates of DOA $\hat{\boldsymbol{\theta}} = [\hat{\theta}_{e1}, \ldots, \hat{\theta}_{ek}, \ldots, \hat{\theta}_{eK}]$ and $\hat{\mathbf{\Phi}} = [\hat{\phi}_{a1}, \ldots, \hat{\phi}_{ak}, \ldots, \hat{\phi}_{aK}]$ do not correspond, the corresponding array manifold are $\hat{\mathbf{G}} = [\mathbf{g}(\hat{\theta}_{a1}), \ldots, \mathbf{g}(\hat{\theta}_{ak}), \ldots, \mathbf{g}(\hat{\theta}_{aK})]$ and $\hat{\mathbf{A}} = [\mathbf{a}(\hat{\phi}_{e1}), \ldots, \mathbf{a}(\hat{\phi}_{ek}), \ldots, \mathbf{a}(\hat{\phi}_{eK})]$, where $k = 1, 2, \ldots, K$.

2) Calculate matrix $\boldsymbol{\psi} = [(\hat{\mathbf{A}})^{+}]_{k,:}\mathbf{R}_{xz}(\hat{\mathbf{G}}^{\mathrm{H}})^{+}$, find the position n of the largest element in $\boldsymbol{\psi}$, and then $\hat{\theta}_{ek}$ and $\hat{\phi}_{an}$ are matched. Let $\hat{\theta}_{ek} = \bar{\theta}_k$ and $\hat{\phi}_{an} = \bar{\phi}_k$, that is, $\bar{\theta}_k$ and $\bar{\phi}_k$ correspond to the elevation and azimuth of the same signal, where $[(\hat{\mathbf{A}})^{+}] = ((\hat{\mathbf{A}})^{\mathrm{H}}(\hat{\mathbf{A}}))^{-1}(\hat{\mathbf{A}})^{\mathrm{H}}$, $[(\hat{\mathbf{A}})^{+}]_{k,:}$ is row k of $[(\hat{\mathbf{A}})^{+}]$, $[(\hat{\mathbf{G}}^{\mathrm{H}})^{+}] = ((\hat{\mathbf{G}})(\hat{\mathbf{G}}^{\mathrm{H}}))^{-1}(\hat{\mathbf{G}})$, and $\mathbf{R}_{xz} = \mathrm{E}[\mathbf{x}(t)\,\mathbf{z}^{\mathrm{H}}(t)]$ is the cross covariance matrix of the received data of the sub-arrays of the proposed algorithm.

B. ALGORITHM COMPLEXITY ANALYSIS

The computational complexity of the proposed algorithm is compared with that of the other four algorithms to verify the effectiveness of the algorithm. The computational complexity is divided into the main computational overhead and the main time complexity, where M and N are the numbers of subarray elements, L is the number of snapshots, $\bar{N}$ is the rank of the full-rank matrix $\mathbf{W}$, and s represents the search steps of the spectral peak search algorithm. In general, $s \gg M$, $s \gg N$, and $s > L$.

From Table 1, we can see that joint SVD has higher computational complexity than other algorithms because it includes the spectral peak search. CMM-ESPRIT does not have high computational complexity caused by peak searching or iterations, however, like the Root-MUSIC and Li algorithms, its covariance matrix needs to be eigen-decomposed or singular value decomposed to get signal subspace or noise subspace, which will lead to a rapid increase in the computational complexity of the algorithm in cases where there are many antennas or sampling points. Compared with the Root-MUSIC algorithm, the Li algorithm has a lower computational complexity than the Root-MUSIC algorithm because it does not require pairing. The proposed method does not need eigen-decomposition to get the signal subspace and does not need peak search to estimate angles. In the case of small antenna numbers or sampling points, the proposed algorithm has no obvious advantage over other algorithms. However, when the number of antennas increases significantly, the proposed algorithm can greatly reduce the computational complexity and hardware cost.

TABLE 1. Comparison of computational cost and complexity.

Methods	Main computational overhead	Major computational complexity
CMM-ESPRIT [21]	Correlation matrix R + EVD of R	$O(MNL + M^3 + N^3 + K^3)$
Root-MUSIC [17]	Correlation matrix R +EVD of R + root finding	$O((M+N)^2L + (M+N)^3 + (M+N)^2K + (M+N))$
Joint SVD [20]	Correlation matrix R + EVD of R + peak search	$O(MNL + N^3 + sN)$
Li method [22]	Correlation matrix R+ EVD of R + root finding	$O((M+N)^2L + (M+N)^3 + (M+N)^2K + M)$
Proposed method	Correlation matrix R+ auxiliary operator Q	$O(MNL + \bar{N}^2K + K^3)$

VI. SIMULATION RESULTS AND ANALYSIS

Simulation experiments are used to verify the feasibility of the algorithm. The input signals are assumed to be far-field narrow-band signals. For simplicity, the incident signals are given according to the traditional definition.

The array simulation conditions are as follows: the x-axis and z-axis sub-array position vectors of the proposed non-uniform L-shaped array are both $D = d \times [0, 1, 2, 5, 9, 11]$, $d = \lambda/2$, the number of each sub-array elements is $N = 6$. In other words, the position coordinates of the proposed non-uniform L-shaped array with eleven elements is (0,0,0), (d,0,0), (2d,0,0), (5d,0,0), (9d,0,0), (11d,0,0), (0,0,d), (0,0,2d), (0,0,5d), (0,0,9d) and (0,0,11d). As a comparison, the position coordinates of the uniform L-shaped array with eleven elements is (0,0,0), (d,0,0), (2d,0,0), (3d,0,0), (4d,0,0), (5d,0,0), (0,0,d), (0,0,2d), (0,0,3d), (0,0,4d) and (0,0,5d).

Simulation 1: For the proposed non-uniform L-shaped array and uniform L-shaped array with eleven elements, two kinds of array power patterns are given. When the elevation and azimuth of the beam incidence are $(\theta_0, \phi_0) = (0, 0)$, the array pattern is as shown in Figure 4.

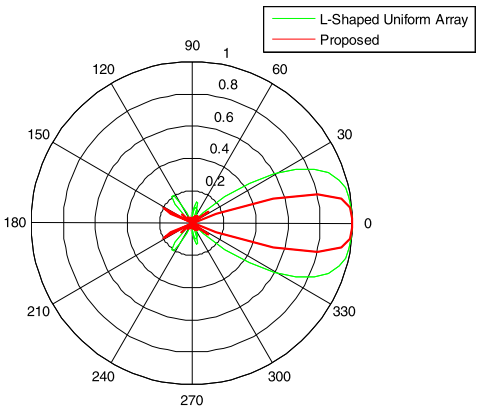

FIGURE 4. Power pattern of the proposed and uniform L-shaped array.

From Figure 4, it can be seen that the main lobe beam width of the proposed eleven-element array is narrower than that of the eleven-element uniform L-shaped array. The non-uniform L-shaped array adopted in this paper not only has the estimation performance of the nested array, but it also does not need to be composed of two or more uniform linear subarrays. The proposed non-uniform L-shaped array is more flexible in terms of the array arrangement compared with the nested array, and it has a stronger DOA estimation capability compared with the uniform L-shaped array because of its narrower beam width and better array pointing ability.

The angle resolution of the array is an important index to estimate the DOA. The smaller the angle difference that the array can resolve is, the higher the resolution of the array is. Therefore, when the SNR is set to 10 dB, the number of snapshots is 2000, the incident angle is $(\theta_1, \phi_1) = (20°, 30°)$, the difference between the other incident angle and the first incident angle changes from 1° to 20°, the minimum angle difference that can be resolved by the proposed non-uniform L-shaped array and the uniform L-shaped array is as shown in Figure 5.

Figure 5 plots the variation curve of root-mean-square error (RMSE) of two-dimensional DOA estimation versus the angle difference. It can also be seen from Figure 5 that the angular resolution of the proposed six-element array is better than that of the six-element uniform L-shaped array, because the angular resolution of the array is directly related to the array aperture, while the array aperture is related to the number of array elements and the spacing of the array elements. When the number of array elements is the same, the proposed non-uniform L-shaped array enlarges the spacing of array elements and expands the array aperture, so the resolution of the proposed non-uniform L-shaped array is superior to that of the uniform L-shaped array.

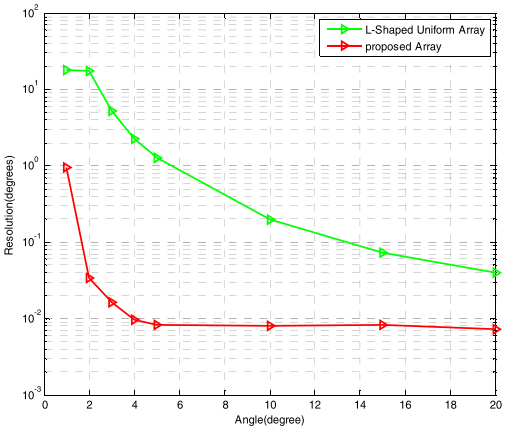

FIGURE 5. The variation curve of RMSE of two-dimensional DOA estimation versus the angle difference.

Simulation 2: There are $K = 10$ far-field narrow-band signals incident on the proposed non-uniform L-shaped array and uniform L-shaped array, the incident angles are $(\theta_1, \phi_1) = (20°, 20°), (\theta_2, \phi_2) = (30°, 30°), (\theta_3, \phi_3) = (50°, 50°), (\theta_4, \phi_4) = (60°, 60°), (\theta_5, \phi_5) = (80°, 80°), (\theta_6, \phi_6) = (90°, 90°), (\theta_7, \phi_7) = (100°, 100°), (\theta_8, \phi_8) = (120°, 120°), (\theta_9, \phi_9) = (130°, 130°), (\theta_{10}, \phi_{10}) = (150°, 150°)$ respectively. The simulation result when the signal-to-noise ratio (SNR) is 10 dB and the number of snapshots is L = 2000 is shown in Figure 6.

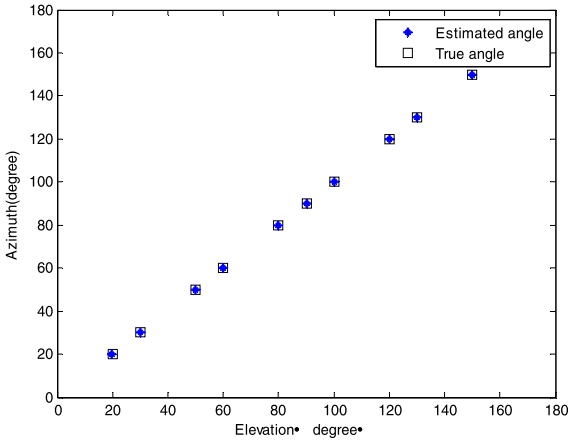

FIGURE 6. Two-dimensional DOA estimation of spatial objects.

From Figure 6, it can be seen that the proposed algorithm in this paper can correctly identify 10 spatial targets under a low SNR with a small angle deviation. When the number of signal sources is more than the number of elements, this algorithm has high estimation accuracy.

In order to further reflect that the method proposed in this paper can estimate short-range spatial targets, the direction finding of K = 2 far-field narrow-band targets is carried out, and the incident angles are $(\theta_1, \phi_1) = (61°, 81°)$ and $(\theta_2, \phi_2) = (62°, 82°)$ respectively. The simulation result when the signal-to-noise ratio is 20 dB and the number of

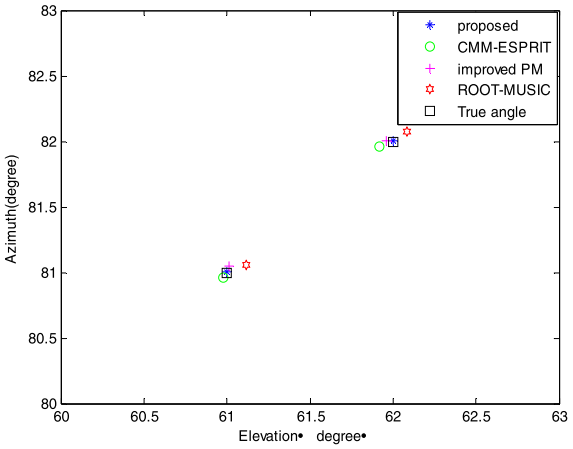

FIGURE 7. The two-dimensional DOA estimation of a nearby target.

snapshots is L = 2000 is shown in Figure 7. The proposed algorithm and other algorithms all adopt the non-uniform L-shaped array.

Figure 7 shows a comparison of the performance of the proposed algorithm versus other algorithms such as the Root-MUSIC algorithm [17], CMM-ESPRIT algorithm [21], and improved PM algorithm [23]. From Figure 7, it can be seen that the proposed algorithm can identify spatial short-range targets, and other algorithms have large estimation errors. Under the same non-uniform L-shaped array, the estimated value of this algorithm is closer to the true value.

Simulation 3: The proposed algorithm was compared with the Root-MUSIC algorithm in [17], the joint SVD algorithm in [20], the CMM-ESPRIT algorithm in [21], and the Li algorithm in [22] under different SNRs. The proposed algorithm adopts the non-uniform L-shaped array and other algorithms adopt the uniform L-shaped array. At the same time, the Cramer-Rao Bound (CRB) in [32] of the two arrays are given. Two narrow-band far-field targets are identified in space, the incident angles of two target sources are $(\theta_1, \phi_1) = (130^\circ, 80^\circ)$ and $(\theta_2, \phi_2) = (70^\circ, 40^\circ)$, and the number of snapshots is L = 2000. The statistical success probability and estimated root-mean-square error of 200 experiments were conducted from 0 to 20 dB, and the results are shown in Figure 8.

In order to better understand the impact of the number of snapshots on the performance of five algorithms, other conditions remain unchanged. The simulation result when the

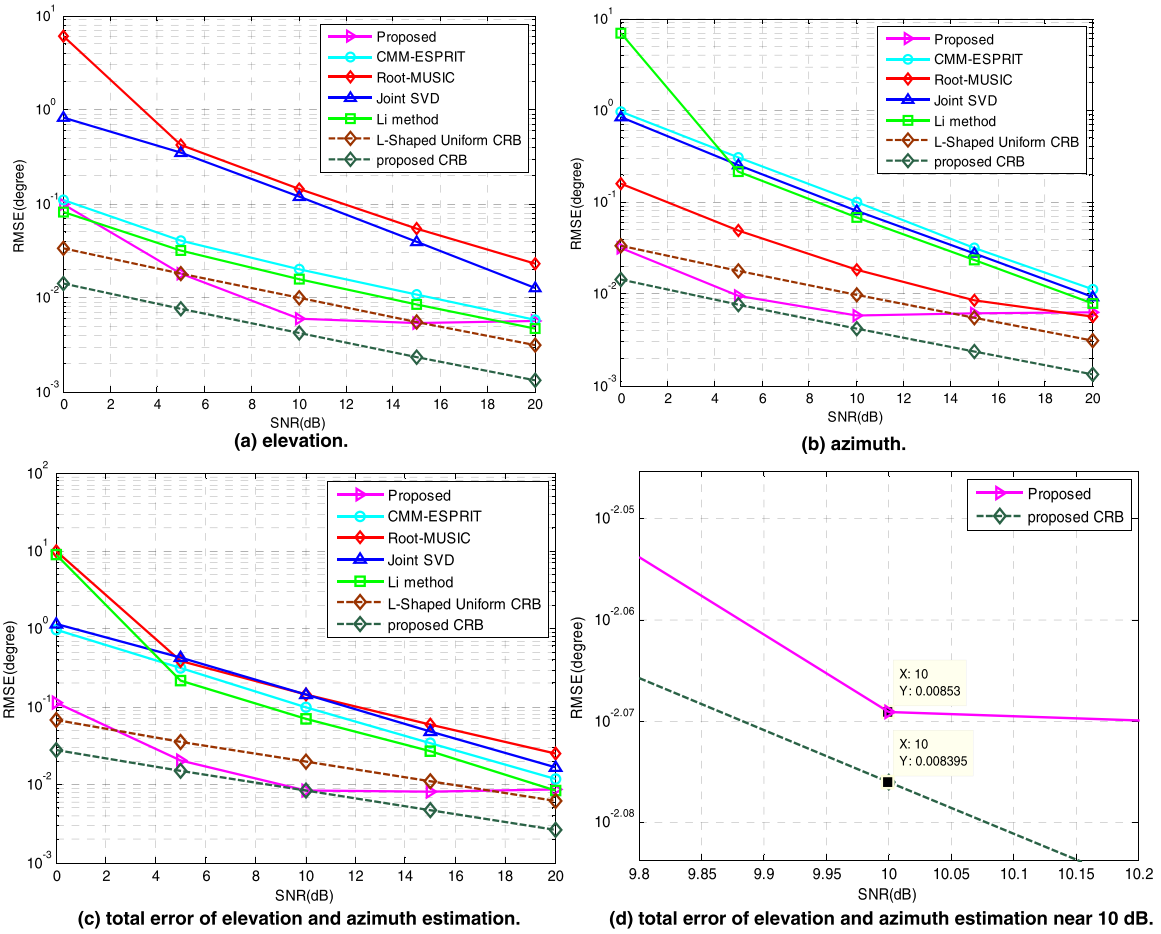

(a) elevation.

(b) azimuth.

(c) total error of elevation and azimuth estimation.

(d) total error of elevation and azimuth estimation near 10 dB.

FIGURE 8. The variation curve of RMSE of two-dimensional DOA estimation versus SNR.

TABLE 2. Specific RMSE values of each algorithm under two SNR.

	SNR = 5 dB		SNR = 15 dB	
	RMSE1	RMSE2	RMSE1	RMSE2
CMM-ESPRIT	0.0336	0.3072	0.0053	0.0334
Root-MUSIC	0.4140	0.0541	0.0583	0.0089
Joint SVD	0.3448	0.2549	0.0392	0.0266
Li method	0.0257	0.2161	0.0057	0.0241
Proposed	0.0180	0.0091	0.0047	0.0060

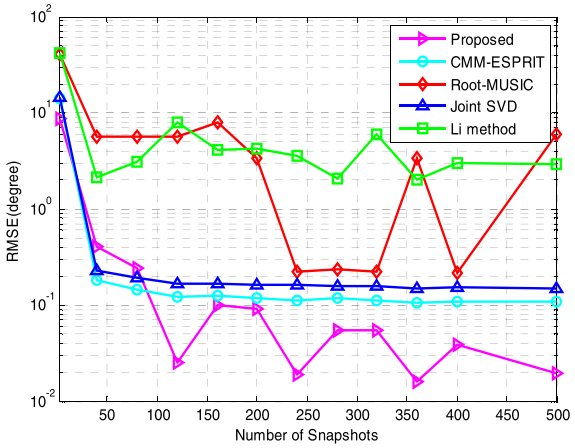

FIGURE 9. The variation curve of RMSE of two-dimensional DOA estimation versus the number of snapshots.

signal-to-noise ratio is 10 dB and the number of snapshots varies from 1 to 500 is shown in Figure 9.

Figure 8 and Figure 9 compare the performance of DOA estimation by the proposed algorithm and other algorithms. In Figure 8, (a) and (b) show the variation curves of the estimation performance of the elevation and azimuth with the SNR, respectively, and (c) shows the variation curves of the total estimation error with the SNR. It can be seen that the proposed algorithm has the highest accuracy and the smallest error, followed by the Li algorithm and CMM-ESPRIT algorithm, while the joint SVD and Root-MUSIC algorithm perform poorly. With an increase in the SNR, the estimation performance of the algorithms increases obviously. When the SNR is close to 20 dB, several algorithms can achieve a rather high DOA estimation accuracy. In order to further clarify the accuracy of the proposed algorithm, RMSE values of elevation and azimuth are shown in table 2 when SNR = 5dB and SNR = 15dB. It can be clearly seen from table 2 that the proposed algorithm is better than other algorithms. Figure 9 shows the variation curve of the RMSE of two-dimensional DOA estimation versus the number of snapshots. It can be seen that when the number of snapshots is small, the root mean square error of the algorithm in this paper is the smallest and the performance is the best, followed by the joint SVD algorithm and CMM-ESPRIT algorithm, while Li algorithm and Root-MUSIC algorithm

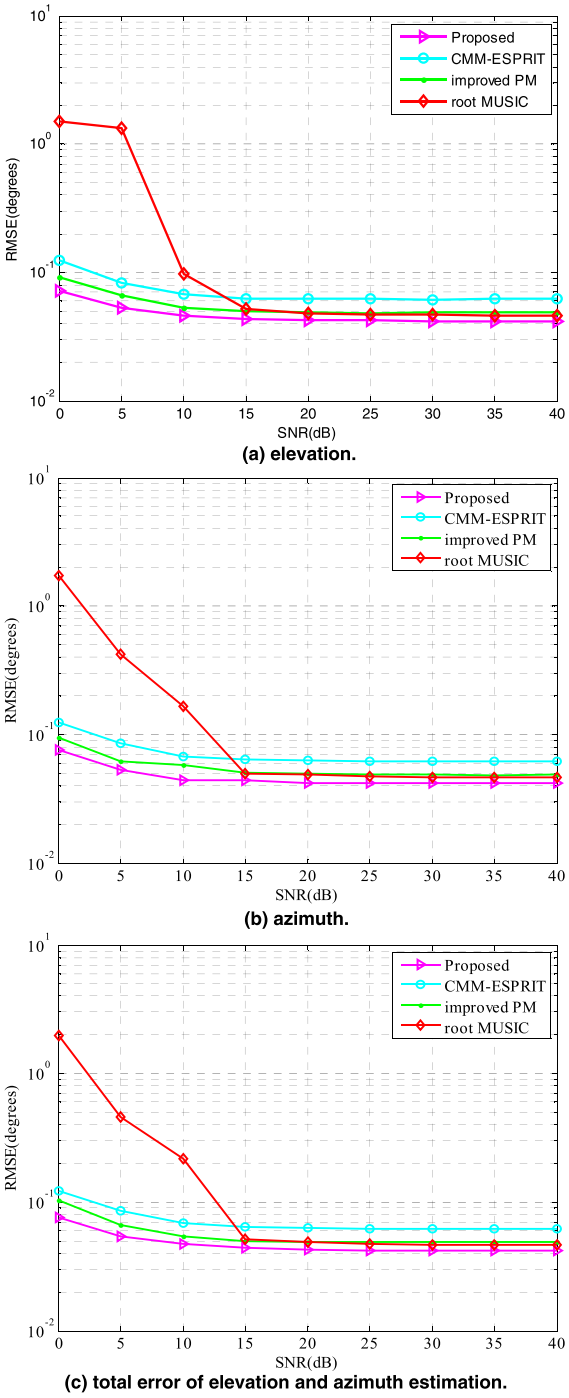

FIGURE 10. RMSE of four algorithms versus SNR under the same non-uniform L-shaped array.

perform poorly. When the number of snapshots is more than 50, the algorithm performance tends to be stable.

Simulation 4: In order to verify the effectiveness of the proposed algorithm in the same array, the proposed algorithm was compared with the Root-MUSIC algorithm, the improved PM algorithm, and the CMM-ESPRIT algorithm under different SNRs. The receiving arrays of all four algorithms are all configured as the proposed non-uniform

L-shaped array, in other words, the array element number, array arrangement and array aperture are exactly the same. It should be noted that Li algorithm [22] and joint SVD algorithm [20] are not suitable for DOA estimation under non-uniform array in the paper, so they do not participate in the comparison. Ten uncorrelated equal-powered signals with the following parameter values, $(\theta_1, \phi_1) = (20°, 20°)$, $(\theta_2, \phi_2) = (30°, 30°)$, $(\theta_3, \phi_3) = (50°, 50°)$, $(\theta_4, \phi_4) = (60°, 60°)$, $(\theta_5, \phi_5) = (80°, 80°)$, $(\theta_6, \phi_6) = (90°, 90°)$, $(\theta_7, \phi_7) = (100°, 100°)$, $(\theta_8, \phi_8) = (120°, 120°)$, $(\theta_9, \phi_9) = (130°, 130°)$ and $(\theta_{10}, \phi_{10}) = (150°, 150°)$, impinge upon the receiving array, 2000 snapshots are used for 200 Monte Carlo simulation experiments. SNR is set to range between 0 and 40 dB. The results are shown in Figure 10. In order to better understand the impact of the number of snapshots on the performance of four algorithms, other conditions remain unchanged. The simulation result when the signal-to-noise ratio is 10 dB and the number of snapshots varies from 1 to 500 is shown in Figure 11.

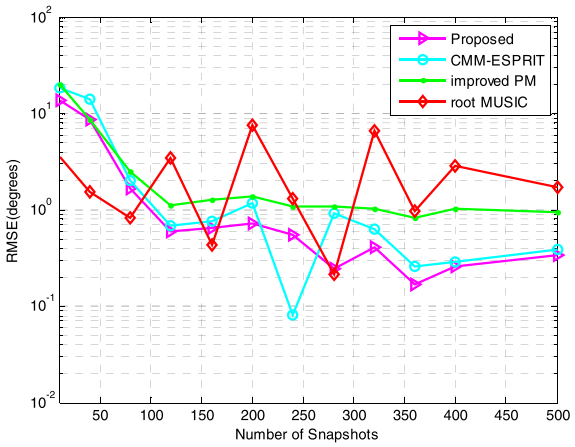

FIGURE 11. RMSE of four algorithms versus different snapshots under the same non-uniform L-shaped array.

Figure 10 shows a comparison of RMSE of the proposed algorithm versus other algorithms such as the Root-MUSIC algorithm, joint improved PM algorithm and CMM-ESPRIT algorithm. From Figure 10, it is clear that the DOA estimation performance of the proposed algorithm is better than that of other algorithms when the number of signal sources is more than the number of elements. And from the complexity analysis in the previous section, it can be seen that the proposed algorithm has lower computational complexity, so the practical application ability is stronger. Figure 11 shows the comparison of the RMSE of the four algorithms under the same array as the number of snapshots increases. When the number of snapshots is less than 80, the RMSE of the Root-MUSIC algorithm is the smallest, followed by the algorithm in this paper, but when the number of snapshots is greater than 80, the error of the algorithm in this paper is the smallest and the change is gentle, while the RMSE of Root-MUSIC algorithm changes too much. So the simulation results of the four algorithms show that the algorithm in this paper has the best simulation performance.

VII. CONCLUSION

In the case of airborne radar or limited physical space, a kind of non-uniform array is proposed to solve the problem of the existing nested array not being flexible. The array structure does not need to be composed of two or more uniform linear subarrays on the premise of maintaining the same degree of freedom as the nested array. In order to reduce the computational complexity, an auxiliary operator is constructed to obtain the signal subspace under the condition of having many array elements and a large number of snapshots. Finally, the estimation value of the two-dimensional DOA is obtained through ESPRIT-based algorithm. The proposed method not only reduces the number of array elements and improves the accuracy of DOA estimation, but it also has lower computational complexity than the traditional method.

ACKNOWLEDGMENT

The authors would like to thank the anonymous reviewers and the associated editor for their valuable comments and suggestions that improved the clarity of this manuscript. In the course of writing this paper, the authors also owed great thanks to other member of the workgroup for their constant help.

REFERENCES

[1] Z. Zheng, Y. Yang, W.-Q. Wang, G. Li, J. Yang, and Y. Ge, "2-D DOA estimation of multiple signals based on sparse L-shaped array," in *Proc. ISAP*, Okinawa, Japan, Oct. 2016, pp. 1014–1015.
[2] F. Wen, J. Shi, and Z. Zhang, "Closed-form estimation algorithm for EMVS-MIMO radar with arbitrary sensor geometry," *Signal Process.*, vol. 186, Sep. 2021, Art. no. 108117.
[3] X. Wu, W.-P. Zhu, and J. Yan, "A fast gridless covariance matrix reconstruction method for one- and two-dimensional direction-of-arrival estimation," *IEEE Sensors J.*, vol. 17, no. 15, pp. 4916–4927, Aug. 2017.
[4] X. Wang, M. Huang, and L. Wan, "Joint 2D-DOD and 2D-DOA estimation for coprime EMVS–MIMO radar," *Circuits, Syst., Signal Process.*, vol. 40, no. 6, pp. 2950–2966, Jun. 2021.
[5] C. Zhou, Y. Gu, X. Fan, Z. Shi, G. Mao, and Y. D. Zhang, "Direction-of-arrival estimation for coprime array via virtual array interpolation," *IEEE Trans. Signal Process.*, vol. 66, no. 22, pp. 5956–5971, Nov. 2018.
[6] P. Pal and P. P. Vaidyanathan, "Nested array: A novel approach to array processing with enhanced degrees of freedom," *IEEE Trans. Signal Process.*, vol. 58, no. 8, pp. 4167–4181, Aug. 2010.
[7] P. Pal and P. P. Vaidyanathan, "Nested arrays in two dimensions, part I: Geometrical considerations," *IEEE Trans. Signal Process.*, vol. 60, no. 9, pp. 4694–4705, Sep. 2012.
[8] C.-L. Liu and P. P. Vaidyanathan, "Super nested arrays: Linear sparse arrays with reduced mutual coupling—Part I: Fundamentals," *IEEE Trans. Signal Process.*, vol. 64, no. 15, pp. 3997–4012, Aug. 2016.
[9] P. Pal and P. P. Vaidyanathan, "Multiple level nested array: An efficient geometry for 2qth order cumulant based array processing," *IEEE Trans. Signal Process.*, vol. 60, no. 3, pp. 1253–1269, Mar. 2012.
[10] L. Yuki and I. Koichi, "Extension of two-level nested array with larger aperture and more degrees of freedom," in *Proc. Int. Symp. Antennas Propag.*, Okinawa, Japan, Oct. 2016, pp. 442–443.
[11] L. Wang, Z. Hui, S. Wang, and G. Wang, "Underdetermined DOA estimation algorithm based on an improved nested array," *Wireless Pers. Commun.*, vol. 112, no. 4, pp. 2423–2437, Jan. 2020.
[12] J. Li and R. T. Compton, "Angle and polarization estimation using ESPRIT with a polarization sensitive array," *IEEE Trans. Antennas Propag.*, vol. 39, no. 9, pp. 1376–1383, Sep. 1991.

[13] M. D. Zoltowski and K. T. Wong, "Self-initiating MUSIC-based direction finding and polarization estimation in spatio-polarizational beamspace," *IEEE Trans. Antennas Propag.*, vol. 48, no. 8, pp. 1235–1245, Aug. 2000.
[14] M. Wax, T. J. Shan, and T. Kailath, "Spatial-temporal spectral analysis by eigenstructure method," *IEEE Trans. Acoust. Speech Signal Process.*, vol. ASSP-32, no. 4, pp. 817–827, Sep. 1984.
[15] X. Yuan, "Quad compositions of collocated dipoles and loops: For direction finding and polarization estimation," *IEEE Antennas Wireless Propag. Lett.*, vol. 11, pp. 1044–1047, Aug. 2012.
[16] X. Yuan, K. T. Wong, and K. Agrawal, "Polarization estimation with a dipole-dipole pair, a dipole-loop pair, or a loop-loop pair of various orientations," *IEEE Trans. Antennas Propag.*, vol. 60, no. 5, pp. 2442–2452, May 2012.
[17] K. T. Wong, L. S. Li, and M. D. Zoltowski, "Root-MUSIC-based direction-finding and polarization estimation using diversely polarized possibly collocated antennas," *IEEE Antenn Wireless Propag. Lett.*, vol. 3, pp. 129–132, 2004.
[18] J. Li, X. Zhang, and H. Chen, "Improved two-dimensional DOA estimation algorithm for two-parallel uniform linear arrays using propagator method," *Signal Process.*, vol. 92, no. 12, pp. 3032–3038, Dec. 2012.
[19] L. Wang, L. Yang, G. Wang, and S. Wang, "DOA and polarization estimation based on sparse COLD array," *Wireless Pers. Commun.*, vol. 85, no. 4, pp. 2447–2462, Jul. 2015.
[20] J.-F. Gu and P. Wei, "Joint SVD of two cross-correlation matrices to achieve automatic pairing in 2-D angle estimation problems," *IEEE Antennas Wireless Propag. Lett.*, vol. 6, pp. 553–556, 2007.
[21] S. Kikuchi, H. Tsuji, and A. Sano, "Pair-matching method for estimating 2-D angle of arrival with a cross-correlation matrix," *IEEE Antennas Wireless Propag. Lett.*, vol. 5, pp. 35–40, 2006.
[22] J. Li and D. Jiang, "Joint elevation and azimuth angles estimation for L-shaped array," *IEEE Antennas Wireless Propag. Lett.*, vol. 16, pp. 453–456, 2017.
[23] L. Xu, R. Wu, X. Zhang, and Z. Shi, "Efficient 2-D DOA and frequency estimation for L-shaped array via RD-PM," *Int. J. Electron.*, vol. 106, no. 9, pp. 1394–1411, Sep. 2019.
[24] Z. Zheng and S. Mu, "Two-dimensional DOA estimation using two parallel nested arrays," *IEEE Commun. Lett.*, vol. 24, no. 3, pp. 568–571, Mar. 2020.
[25] Z. Zheng, Y. Huang, W.-Q. Wang, and H. C. So, "Direction-of-arrival estimation of coherent signals via coprime array interpolation," *IEEE Signal Process. Lett.*, vol. 27, pp. 585–589, 2020.
[26] A. Lu, Y. Guo, and N. Li, "Efficient gridless 2-D direction-of-arrival estimation for coprime array based on decoupled atomic norm minimization," *IEEE Access*, vol. 8, pp. 57786–57795, 2020.
[27] X. Zhang, W. Zheng, W. Chen, and Z. Shi, "Two-dimensional DOA estimation for generalized coprime planar arrays: A fast-convergence trilinear decomposition approach," *Multidimensional Syst. Signal Process.*, vol. 30, no. 1, pp. 239–256, Jan. 2019.
[28] X. Wang, L. Wan, M. Huang, C. Shen, Z. Han, and T. Zhu, "Low-complexity channel estimation for circular and noncircular signals in virtual MIMO vehicle communication systems," *IEEE Trans. Veh. Technol.*, vol. 69, no. 4, pp. 3916–3928, Apr. 2020.
[29] H. Chen, C. Hou, W.-P. Zhu, W. Liu, Y.-Y. Dong, Z. Peng, and Q. Wang, "ESPRIT-like two-dimensional direction finding for mixed circular and strictly noncircular sources based on joint diagonalization," *Signal Process.*, vol. 141, pp. 48–56, Dec. 2017.
[30] T. Ahmed and X. Zhang, "Higher-order unitary propagator method for 2D-DOA estimation of non-circular sources via uniform rectangular array," *Digit. Signal Process.*, vol. 100, May 2017, Art. no. 102700.
[31] Y. Yang, X. Mao, and Y. Hou, "2-D DOA estimation via correlation matrix reconstruction for nested L-shaped array," *Digit. Signal Process.*, vol. 98, Mar. 2020, Art. no. 102623.
[32] C.-L. Liu and P. P. Vaidyanathan, "Cramér–Rao bounds for coprime and other sparse arrays, which find more sources than sensors," *Digit. Signal Process.*, vol. 61, pp. 43–61, Feb. 2017.

GUIBAO WANG received the Master of Science degree in computational mathematics and the Ph.D. degree in information engineering from Xidian University, Xi'an, China, in 2003 and 2014, respectively. He was a Professor with the School of Physics and Telecommunication Engineering, Shaanxi University of Technology, China. His research interest includes polarization sensitive array signal processing.

PEIYAO ZHAO was born in Shaanxi, China, in October 2000. She is currently pursuing the bachelor's degree with the School of Communication Engineering, Xidian University, Xi'an, China. Her research interests include signal processing and knowledge graph.

LE WANG was born in Henan, China, in July 1997. She is currently pursuing the master's degree in radio physics with Xidian University, Xi'an, China. Her research interest includes sparse array processing and direction of arrival estimation based on non-uniform array.

LANMEI WANG received the Master of Science degree in radio physics and the Ph.D. degree in information engineering from Xidian University, Xi'an, China, in 2002 and 2005, respectively. She was a Professor with the School of Physics and Optoelectronic Engineering, Xidian University. Her research interests include polarization sensitive array signal processing and the application of compressed sensing and frame theory in array signal processing.